HAL open science

Multifunctional Amyloid Oligomeric Nanoparticles for Specific Cell Targeting and Drug Delivery

Weiqiang Wang, Rafayel Azizyan, Adriana Garro, Andrey Kajava, Salvador Ventura

To cite this version:

Weiqiang Wang, Rafayel Azizyan, Adriana Garro, Andrey Kajava, Salvador Ventura. Multifunctional Amyloid Oligomeric Nanoparticles for Specific Cell Targeting and Drug Delivery. Biomacromolecules, 2020, 21 (10), pp.4302-4312. 10.1021/acs.biomac.0c01103 . hal-03431802

HAL Id: hal-03431802

https://hal.science/hal-03431802v1

Submitted on 17 Nov 2021

HAL is a multi-disciplinary open access archive for the deposit and dissemination of scientific research documents, whether they are published or not. The documents may come from teaching and research institutions in France or abroad, or from public or private research centers.

L'archive ouverte pluridisciplinaire **HAL**, est destinée au dépôt et à la diffusion de documents scientifiques de niveau recherche, publiés ou non, émanant des établissements d'enseignement et de recherche français ou étrangers, des laboratoires publics ou privés.

Biomacromolecules

pubs.acs.org/Biomac Article

Multifunctional Amyloid Oligomeric Nanoparticles for Specific Cell Targeting and Drug Delivery

Weiqiang Wang, Rafayel A. Azizyan, Adriana Garro, Andrey V. Kajava, and Salvador Ventura*

Cite This: https://dx.doi.org/10.1021/acs.biomac.0c01103 Read Online

ACCESS | Metrics & More | Article Recommendations | Supporting Information

ABSTRACT: Natural selection has endorsed proteins with amazing structures and functionalities that cannot be matched by synthetic means, explaining the exponential interest in developing protein-based materials. Protein self-assembly allows fabricating complex supramolecular structures from relatively simple building blocks, a bottom-up strategy naturally employed by amyloid fibrils. However, the design of amyloid-inspired materials with biological activity is inherently difficult. Here, we exploit a modular procedure to generate functional amyloid nanostructures with tight control of their mesoscopic properties. The soft amyloid core of a yeast prion was fused to dihydrofolate reductase through flexible linkers of different sizes. This enabled us to produce, for the first time, biocompatible protein-only amyloid-like oligomeric nanoparticles with defined dimensions in which the embedded enzyme remained highly active, as assessed by biophysical and enzymatic assays. The modular design allowed one to obtain multifunctional nanoparticles by incorporating the antibody-binding Z-domain to the protein fusion. We show how these assemblies can be exploited for antibody-directed targeting of specific cell types and the localized delivery of methotrexate, resulting in the intracellular uptake of the drug by cancer cells and their death. Overall, the novel protein particles we describe in this work might find applications in areas as diverse as biocatalysis, bioimaging, or targeted therapies.

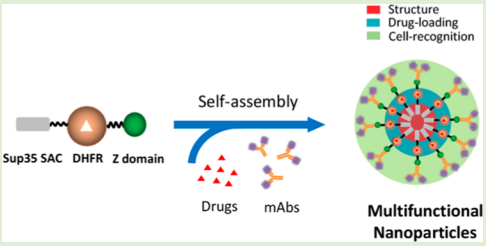

INTRODUCTION

The design and production of biologically inspired assemblies that can be exploited for the fabrication of functional materials is a rapidly growing area of research.[1] Amyloid fibrils have been traditionally associated with human diseases.[2] However, the recent discovery of amyloids assisting biological functions in a wide range of organisms, from bacteria to humans,[3] has changed this perception and inspired the use of their unique architecture to build up nanostructured materials for applications in biomedicine and biotechnology.[4]

A majority of the available amyloid-based functional nanomaterials result from the self-assembly of short synthetic peptides of natural or artificial origin.[5] In contrast, the assembly of globular proteins into amyloid-like materials with biological activity has been less successful. This is expected since the aggregation of globular domains into amyloid structures necessarily implies a process of conformational conversion in which they lose their native fold and thus their activity.[6]

The main advantage of protein-based materials is the nature of globular proteins, which allows one to alter the material functionality by genetic redesign to fit the intended application. We have recently succeeded in designing highly ordered amyloid-like nanofibrils containing properly folded and highly active proteins using a modular strategy.[7] The distinctive feature of the approach consists in the use of a soft amyloid core (SAC) as the assembling unit. SACs are short amyloidogenic sequence stretches initially identified in the disordered and low-complexity domains of yeast prions.[8] They differ from the classical amyloid cores of pathogenic proteins in that they are slightly longer and more polar.[9,10] This results in a weaker and more diffuse amyloid propensity but still sufficient to nucleate the self-assembly reaction. The SAC is fused through a Gly/Ser soluble and flexible linker to the globular protein of interest. The resulting fusion proteins are produced recombinantly at high yield and in a soluble manner; still, their ordered aggregation can be induced under defined conditions, rendering functional synthetic amyloid fibrils in which the SAC forms the amyloid spine and the globular domains hang from it in an active conformation, as demonstrated for fluorescent proteins and enzymes.[7]

We use the SAC (residues 100−118) of the Sup35 yeast prion (Sup35-SAC) as the default assembling module. Its small size allows one to use a connecting linker of only eight residues and obtain amyloid fibrils in which the fused protein is active without major steric impediments and with a reduced entropy penalization for the assembly reaction. This is in contrast with natural amyloid proteins displaying a similar architecture, like

Received: July 21, 2020
Revised: September 1, 2020
Published: September 4, 2020

 © XXXX American Chemical Society

the prion proteins Het-s,[11] Sup35p, and Ure2p,[12] human Rip1/Rip3,[13] or the TAR-DNA binding proteins,[14] where the connecting linker is significantly longer (>50 residues).

Recently, using molecular and mesoscopic modeling, we were able to establish a theoretical relationship between the size of a globular domain and the length of the shortest linker that still allows the formation of infinite amyloid fibrils when fused to an amyloidogenic sequence.[15] The model suggested that shortening the linker below this size limit would result in the formation of oligomers of defined size instead of the typical fibrils.[16,17] This might provide a unique opportunity to generate small protein-based nanoparticles decorated with *à la carte* globular protein functionalities.

Here, we connected Sup35-SAC to the dihydrofolate reductase (DHFR) enzyme[18] (Sup35-DHFR) and demonstrate that we can control the mesoscopic properties of the resulting assemblies just by playing with the linker length, obtaining either catalytic fibrils or catalytic oligomeric nanoparticles. These nanoparticles are spherical assemblies of an amyloid-like nature but devoid of any toxicity. They are homogenous in size, stable, and more active than the corresponding fibrils.

We explored the potential of these novel protein-based nanoparticles to generate functionalized materials by creating a tripartite fusion in which we incorporated the Z-domain,[19] an engineered analog of the B-domain of the *Staphylococcus aureus* protein A[20] to the C-terminus of the Sup35-DHFR protein. The new fusion protein also assembles into spherical oligomeric nanoparticles that can now be decorated with any antibody of interest, thanks to the Z-domain's nanomolar affinity for antibodies' Fc domains, thus generating multivalent particles.

We show that antibody-loaded nanoparticles can be directed specifically against cancer cells and demonstrate that they can be used as nanocarriers for cell-specific delivery of methotrexate (MTX). MTX acts as an antagonist of folic acid, which is necessary for DNA synthesis and accordingly is used as a chemotherapeutic agent for the treatment of cancer.[21,22] However, it displays a weak pharmacokinetic profile, and significant off-target toxicity[23−25] and MTX-based nanomedicines have been designed to overcome these drawbacks.[26] In our nanoparticles, the Z-domain-bound antibody acts as a cellular selector and the DHFR moiety as the MTX carrier. Once released from its carrier, the drug is internalized, displaying a potent and localized cytotoxic effect. The strategy is simple and modular and can be adapted to target any cell type of interest.

■ MATERIALS AND METHODS

Reagents and Enzymes. Reagents and enzymes were purchased from Sigma-Aldrich (U.K.) unless otherwise stated. Carbon grids (400 square mesh copper) were purchased from Micro to Nano (The Netherlands), and the uranyl acetate solution was provided by the microscopy service at Universitat Autònoma de Barcelona. Sup35-SAC peptides were purchased from CASLO ApS (Scion Denmark Technical University).

Expression and Purification of Proteins. The cDNA of Sup35-5aa-DHFR, cloned in the plasmid pET28(a) with a His6 tag, was acquired from GenScript. The constructs pET28(a)/Sup35-8aa-DHFR, pET28(a)/wild-type DHFR (DHFR-wt), and pET28(a)/Sup35-5aa-DHFR-Z were obtained by mutagenesis on top of the plasmid pET28(a)/Sup35-5aa-DHFR. *Escherichia coli* BL21 (DE3)-competent cells were transformed with the corresponding plasmids. Then, transformed cells were grown in a 10 mL lysogeny broth (LB) medium containing 50 $\mu g \cdot mL^{-1}$ kanamycin, overnight at 37 °C and transferred into 1 L fresh LB media containing 50 $\mu g \cdot mL^{-1}$ kanamycin. After reaching an OD_{600} of 0.6, the culture was induced with 0.4 mM isopropyl β-D-1-thiogalactopyranoside (IPTG) and grown at 20 °C for 16 h. Cells were collected by centrifugation at 5000 rpm for 15 min at 4 °C. The collected pellet was resuspended into 20 mL of phosphate-buffered saline (PBS) pH 7.4 containing 20 mM imidazole, 1 $mg \cdot mL^{-1}$ lysozyme, and 1 mM PMSF. The solution was incubated on ice, followed by sonication for 20 min. The supernatant was collected by centrifugation at 15 000 rpm for 30 min at 4 °C and purified using a nickel-charged IMAC column, followed by a gel filtration onto a HiLoad Superdex 75 prep-grade column (GE Healthcare). The purified proteins were frozen with liquid nitrogen and stored at −80 °C. Sodium dodecyl sulfate-polyacrylamide gel electrophoresis (SDS-PAGE) confirmed the purity of the samples. The concentrations of the proteins DHFR-wt, Sup35-5aa-DHFR, Sup35-8aa-DHFR, and Sup35-5aa-DHFR-Z were determined by ultraviolet (UV) absorption using ε values of 33 585, 38 055, 38 055, and 39 420 $L \cdot mol^{-1} \cdot cm^{-1}$, respectively.

Conformational Characterization. Proteins were dissolved at a final concentration of 20 μM in PBS pH 7.4 buffer; then, samples were filtered through a 0.22 μm Millipore filter and immediately analyzed. Far-UV circular dichroism (CD) spectra were recorded from 260 to 200 nm at 1 nm bandwidth, with a response time of 1 s and a scan speed of 100 $nm \cdot min^{-1}$ in a Jasco-710 spectropolarimeter (Jasco Corporation, Japan), thermostated at 25 °C. Ten accumulations were averaged for each spectrum.

Aggregation Assay. Proteins were prepared at 200 μM for Sup35-5aa-DHFR and Sup35-8aa-DHFR and at 600 μM for Sup35-5aa-DHFR-Z in PBS pH 7.4 and filtered through a 0.22 μm filter. The samples were incubated at 25 °C, with agitation for four days. DHFR-wt was incubated at the same concentrations and conditions.

Amyloid Dye Binding. Thioflavin-T (Th-T) and Congo red (CR) were used to monitor the formation of amyloid assemblies. For the Th-T binding assay, incubated proteins were diluted to a final concentration of 20 μM in PBS pH 7.4, in the presence of 25 μM Th-T. Emission fluorescence was recorded in the 460−600 nm range, using an excitation wavelength of 445 nm and an emission bandwidth of 5 nm on a Jasco FP-8200 spectrofluorometer (Jasco Corporation, Japan). For the CR binding assay, incubated proteins were prepared at a final concentration of 20 μM and CR was mixed to a final concentration of 20 μM. Absorption spectra were recorded in the range from 375 to 700 nm in a Specord 200 Plus spectrophotometer (Analytik Jena, Germany). Spectra of protein alone and buffer were acquired to subtract their contribution to the signal.

Transmission Electron Microscopy (TEM). For TEM sample preparation, 10 μL of the incubated proteins was deposited on a carbon-coated copper grid for 10 min, and the excess liquid was removed with filter paper, followed by negative staining with 10 μL of 2% (w/v) uranyl acetate for 1 min. Grids were scanned using a JEM 1400 transmission electron microscope (JEOL Ltd., Japan) operating at 80 kV, and images were acquired with a CCD GATAN ES1000W Erlangshen camera (Gatan Inc.). The particles' diameter was analyzed with Image J software (National Health Institute), averaging the measures of 100 individual particles.

Scanning Electron Microscopy (SEM). A sample of 50 μL of incubated protein was centrifuged, and the resulting supernatant was removed. The precipitate was resuspended in 50 μL of water and washed twice to remove salt traces. Then, 5 μL of the resuspension was deposited on a silicon slice (0.5 cm × 0.5 cm) and dried with nitrogen flow. Silicon slices were scanned using a Merlin field-emission scanning electron microscope (Zeiss Ltd., Germany) at 2 kV, and images were acquired with an in-lens SE detector. The diameter of the particles was calculated with Image J (National Health Institute), averaging the measures of 100 individual particles.

Fourier Transform Infrared (FTIR) Spectroscopy. DHFR-wt was dissolved at 100 μM in PBS, pH 7.4, and filtered through a 0.22 μm filter. Then, 30 μL of the incubated proteins were centrifuged at 12 000*g* for 30 min and resuspended in 10 μL of water. Samples were placed on the attenuated total reflectance (ATR) crystal and dried out

https://dx.doi.org/10.1021/acs.biomac.0c01103
Biomacromolecules XXXX, XXX, XXX−XXX

under a N_2 flow. The experiments were carried out in a Bruker Tensor 27 FTIR (Bruker Optics) supplied with a Specac Golden Gate MKII ATR accessory. Each spectrum consists of 32 acquisitions measured at a resolution of 2 cm^{-1} using the three-term Blackman−Harris Window apodization function. Data was acquired and normalized using OPUS MIR Tensor 27 software (Bruker Optics), with the Min/Max normalization method, which scales spectrum intensities to the effect that the minimum absorbance unit will be 0 and the maximum will be 2. Infrared (IR) spectra were fitted employing a nonlinear peak-fitting equation using Origin 8.5 (OriginLab Corporation).

Fluorescence Microscopy. First, 20 μL of incubated fusion proteins was centrifuged at 12 000*g* for 30 min, and the supernatant was removed. The precipitate was resuspended in PBS pH 7.4 containing 100 μM fMTX (methotrexate labeled with fluorescein, ThermoFisher Scientific) and incubated for 30 min. For the bifunctional fusion protein Sup35-5aa-DHFR-Z, the precipitate was resuspended in PBS pH 7.4 containing 100 μM fMTX and 1 μg of anti-EGFR antibody labeled with Alexa 555 (ThermoFisher Scientific) and incubated for 30 min. Samples were washed three times to remove any unbound fMTX and antibody and then resuspended in PBS to a final volume of 50 μL. Then, 5 μL of the resuspension was dropped onto a clean glass slide (Deltalab, 26 mm × 76 mm) and covered by a cover slide (Deltalab, 22 mm × 22 mm). Fluorescence imaging of particles and fibrils was carried out on an Eclipse 90i epifluorescence optical microscope equipped with a Nikon DXM1200F (Nikon, Japan) camera and ACT-1 software. Images were acquired with an excitation filter of 465−495 nm or 540−580 nm and detecting fluorescence emission in a range of 515−555 nm or 590−630 nm.

Dynamic Light Scattering (DLS). The size of the incubated proteins was determined using a Malvern Zetasizer Nano ZS90 (ATA Scientific, Australia) in PBS buffer, pH 7.4, at 25 °C.

Catalytic Activity of Dihydrofolate Reductase Embedded in Amyloid Assemblies. The Sup35-5aa-DHFR particles and Sup35-8aa-DHFR fibrils were prepared at 2 μM in an activity buffer (0.1 M potassium phosphate, pH 7.4, 1 mM DTT, 0.5 M KCl, 1 mM ethylenediaminetetraacetic acid (EDTA), 20 mM sodium ascorbate). Then, 50 μL of the sample was mixed with 850 μL of activity buffer in a cuvette and preincubated at room temperature for 10 min. The reaction was then initiated by adding 50 μL of 2 mM 7,8-dihydrofolate (DHF) solution and 50 μL of a 2 mM nicotinamide adenine dinucleotide phosphate (NADPH) solution. Sup35-SAC fibrils and lysozyme were used as negative controls. For the determination of the kinetic parameters, a final concentration of 20 nM assemblies and 20 μM of DHF was preincubated in an activity buffer at room temperature. The reaction was initiated by adding NADPH to a final concentration in the range from 10 to 200 μM. The absorbance change at 340 nm was monitored on a Specord 200 Plus spectrophotometer (Analytik Jena, Germany). The initial velocity at each concentration was determined upon fitting the reaction with Origin 8.5 (OriginLab Corporation). The reciprocal of the velocity of the reaction was plotted against the reciprocal of the concentration of NADPH. The catalytic constants V_{max}, K_m, K_{cat}, and K_{cat}/K_m were calculated.

Thermodynamic Dissociation Constants. The equilibrium dissociation constants (K_d) for enzyme−NADPH complexes were determined by fluorescence titration at 25 °C. In particular, the Sup35-5aa-DHFR and Sup35-8aa-DHFR assemblies were prepared at 100 nM in an activity buffer in a quartz cuvette. The titrations were carried out by serial additions of aliquots (1−4 μL) of NADPH into the cuvette. The intrinsic fluorescence spectra in the range from 300 to 400 nm were recorded 2 min after the addition of NADPH, using an excitation wavelength of 290 nm and an emission bandwidth of 5 nm in a Jasco FP-8200 spectrofluorometer (Jasco Corporation, Japan). A standard tryptophan solution was titrated, and the emission was used to correct for the inner filter effect caused by NADPH. The change in intrinsic fluorescence emission at 340 nm was plotted against the NADPH concentration using Origin 8.5 (OriginLab Corporation), and the K_d was calculated from the binding equation.

Preparation of fMTX- or/and Antibody-Loaded Nanoparticles. The incubated protein Sup35-DHFR-Z was precipitated by centrifugation at 13 000 rpm for 30 min. The precipitate was resuspended in PBS buffer pH 7.4 containing 1 μg of antibody or/and 100 μM fMTX (fluorescein-labeled MTX) and then incubated for 30 min. The concentration of nanoparticles was determined by the reduction of absorbance at 280 nm in the supernatant fraction. Three labeling antibodies (ThermoFisher Scientific)—anti-EGFR antibody labeled with Alexa fluor 555, anti-CD3 antibody labeled with Alexa fluor 488, and goat antirabbit antibody labeled with Alexa fluor 555—were used in this study. Then, the antibody or/and fMTX conjugated particles were washed three times with PBS buffer to remove any unbound antibody or/and fMTX and resuspended in PBS buffer. The antibody-loaded nanoparticles (NPs-anti-EGFR and NPs-anti-CD3), fMTX-loaded nanoparticles (NPs-fMTX), and fMTX- and antibody-loaded nanoparticles (NPs-fMTX-anti-EGFR and NPs-fMTX-anti-rabbit) were used for experiments immediately.

Cell Culture. The human HeLa and nontumoral lung MRC-5 cell lines were obtained from the American Type Culture Collection (ATCC). Both cells were maintained in minimum essential medium α media (MEM-α), supplemented with 10% fetal bovine serum (FBS), and incubated at 37 °C with 5% CO_2.

Cytotoxicity Assay. HeLa and MRC-5 cells were seeded on a 96-well plate at a concentration of 3×10^3/well and incubated at 37 °C for 24 h. For HeLa cells, the medium was replaced with 100 μL of fresh medium containing the treatments. Unloaded Sup35-5aa-DHFR-Z particles were assayed in a range of concentrations 0.5−60 μM. MTX-loaded nanoparticles (NPs-MTX), MTX- and anti-EGFR antibody-loaded nanoparticles (NPs-MTX-anti-EGFR), and free MTX were assayed in a concentration range of 2−20 μM. For NPs-MTX-anti-EGFR samples, the medium was removed, and cells were rinsed three times with DPBS buffer after incubation of 20 min. Then, a fresh medium was added. PBS alone was used as the vehicle control and the medium without cells as a blank. A final concentration of 5 $ng \cdot mL^{-1}$ proteinase K was added to the medium to mimic the proteinase-enriched microenvironment of tumor tissues. For MRC-5 cells, the medium was replaced with a fresh medium containing 2−20 μM Sup35-5aa-DHFR-Z nanoparticles, followed by addition of proteinase K to a final concentration of 5 $ng \cdot mL^{-1}$. Each sample was measured in triplicate, and the plate was incubated at 37 °C with 5% CO_2 for 48 h. Then, 10 μL of the PrestoBlue cell viability reagent (ThermoFisher Scientific) was added to each well and incubated for another 1 h. The fluorescence emission was analyzed on a Victor III Multilabel Plate Reader (Perkin Elmer), equipped with a 530/10 nm CW-lamp filter and a 590/20 nm emission filter. The viability of cells was calculated as follows:

$$\text{viability}\ (\%) = (I_{test} - I_{blank})/(I_{control} - I_{blank}) \times 100\%$$

where I_{test}, I_{blank}, and $I_{control}$ are the fluorescence intensities of the test, blank, and control groups, respectively. The significance of the differences between the test groups and the control was analyzed by one-way analysis of variance (ANOVA) using the Origin 8.5 program (OriginLab Corporation).

Confocal Microscopy. HeLa cells were cultured on an 8-well Millicell EZ slide (Millipore, Germany) to a final confluence of 70−80%. Then, the medium was replaced with a fresh medium containing 20 μM NPs-anti-EGFR and NPs-fMTX-anti-EGFR. The slide was incubated at 37 °C, 5% CO_2 for 20 min. The anti-CD3 IgG-loaded nanoparticles (NPs-anti-CD3) were used as a control. For the internalization assay, the medium was replaced with a fresh medium containing 10 μM Free fMTX and fMTX-loaded nanoparticles (NPs-fMTX) preincubated with 50 $ng \cdot mL^{-1}$ proteinase for 5 min followed by addition of EDTA. The slide was incubated at 37 °C, 5% CO_2 for 4 h. Then, the medium was removed. The adherent cells on the slide were rinsed three times with a fresh medium. Cells were stained with CellMask Deep Red (Invitrogen, ThermoFisher Scientific) at a final dilution of 1:1000 for 10 min. The medium was removed and washed three times with PBS buffer. Cells were fixed with 4% paraformaldehyde (PFA) at room temperature for 20 min, followed by a washing step with PBS buffer. Then, 10 μL of the mounting

https://dx.doi.org/10.1021/acs.biomac.0c01103
Biomacromolecules XXXX, XXX, XXX−XXX

medium containing 4′,6-diamidino-2-phenylindole (DAPI) was dropped onto each well of the slide and covered with a coverslip. The slide was imaged on a Leica TCS SP5 confocal microscope (Leica Biosystems, Germany). Images were acquired using 405, 488 nm, or 561 and 633 nm excitation laser for DAPI, Alexa fluor 488, or 555 nm and CellMask Deep Red, respectively.

Flow Cytometry Assay. The NPs-fMTX-anti-EGFR, NPs-fMTX, and NPs-fMTX-antirabbit were prepared as described above. HeLa cells were prepared in PBS buffer pH 7.4 at a final concentration of 1 × 10^6 mL^{-1}. Then, 200 μL of HeLa cells was precipitated and resuspended in 200 μL of PBS buffer containing 20 μM NPs-fMTX-anti-EGFR, NPs-fMTX, and NPs-fMTX-antirabbit, respectively. After 30 min of incubation, the cells were pelleted and washed three times. Then, 200 μL of the cell suspension was analyzed using a FACSCalibur cytometer (BD Biosciences, Becton Dickinson), equipped with a FITC laser. Fluorescence intensities of cell-bound nanoparticles were analyzed and quantitated using FlowJo (BD Biosciences). Cells treated with PBS were used as the control.

Proteinase Digestion of fMTX-Loaded Sup35-DHFR-Z Particles. The fMTX-loaded particles (NPs-fMTX) were resuspended in PBS buffer containing proteinase K at a final concentration of 1 $\mu g \cdot mL^{-1}$. SDS-PAGE was used to analyze the proteolytic progress at 15, 30, and 45 min. The supernatant's fluorescence spectrum was recorded in the 500−600 nm range at different time points, using an excitation wavelength of 488 nm and an emission bandwidth of 5 nm on a Jasco FP-8200 spectrofluorometer (Jasco Corporation, Japan). The emission maximum was plotted as a function of time. The experiment was performed in duplicate. Lysozyme and PBS, instead of proteinase K, were used as negative controls.

■ RESULTS AND DISCUSSION

Self-Assembly of Sup35-8aa-DHFR into Active Amyloid Fibrils. To generate functional amyloid fibrils with a previously unexplored catalytic activity, we fused Sup35-SAC to the *E. coli* DHFR through an 8-residue-long flexible linker consisting of SG_3SG_2S (Sup35-8aa-DHFR) (Figure S1A,B). The size of DHFR (21.5 kDa) is in the range of GFP (27 kDa) and carbonic anhydrase (30 kDa), two proteins that assemble into active amyloid fibrils when fused to Sup35-SAC.[7]

The fusion protein, Sup35-8aa-DHFR, was expressed recombinantly at 64 $mg \cdot L^{-1}$ and located in the soluble cellular fraction, from which we purified it (Figure S1C). We compared the conformational properties of soluble wild-type DHFR (DHFR-wt) and Sup35-8aa-DHFR proteins by far-UV circular dichroism (CD) (Figure 1A). Their spectra were virtually identical, indicating that Sup35-SAC does not induce significant changes in the DHFR structure. Then, we used the amyloid-specific dyes Thioflavin-T (Th-T) and Congo Red (CR) to assess if, despite its solubility, Sup35-8aa-DHFR self-assembles with time into amyloid-like structures. To this aim, we incubated the fusion protein in PBS buffer pH 7.4 at 37 °C for four days. The incubated Sup35-8aa-DHFR protein promoted a substantial increase in the Th-T fluorescence emission signal, whereas DHFR-wt incubated in the same conditions had a negligible effect (Figure 1B). In agreement with these results, CR binding was observed for incubated Sup35-8aa-DHFR, resulting in a red shift of the CR absorption spectrum, while DHFR-wt did not promote any CR spectral change (Figure 1C). Moreover, the Fourier transform infrared (FTIR) absorbance spectrum of incubated Sup35-8aa-DHFR in the amide I region evidenced the existence of a band at 1621 cm^{-1}, which can be assigned to the intermolecular β-sheet structure characteristic of amyloids (Figure 1D and Table S1). This band was absent in the FTIR spectrum of incubated DHFR-wt (Figure S3 and Table S1). The morphological analysis of the two protein solutions by negative staining and

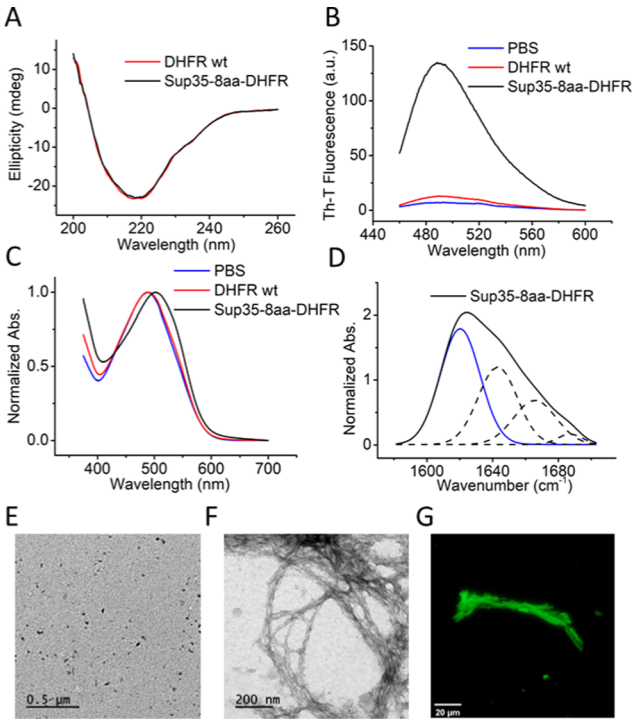

Figure 1. Characterization of soluble and aggregated Sup35-8aa-DHFR. (A) Far-UV CD spectra of soluble Sup35-8aa-DHFR and DHFR-wt, shown in black and red, respectively. Incubated Sup35-8aa-DHFR was analyzed by measuring the Th-T fluorescence emission (B) and CR absorbance (C). DHFR-wt and Sup35-8aa-DHFR are shown in red and black, respectively. PBS without protein was included as a control (blue line). (D) FTIR absorbance spectra of incubated Sup35-8aa-DHFR in the amide I region of the spectrum (solid black line) and the component bands (dashed lines); the intermolecular β-sheet component is shown in blue. (E, F) Representative TEM micrographs of incubated proteins upon negative staining: (E) DHFR-wt and (F) Sup35-8aa-DHFR. Scale bar represents 500 and 200 nm, respectively. (G) Fluorescence microscopy image of Sup35-8aa-DHFR fibrils incubated with fMTX. Scale bar represents 20 μm.

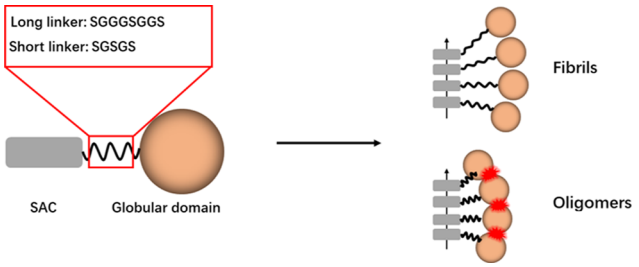

Figure 2. Schematic illustration of the rationale for the formation of stable amyloid oligomers. The scheme of SAC (gray box) is connected with a globular domain (orange ball) by linkers of different lengths. Molecules with long linkers can form infinite amyloid fibrils, whereas those with short linkers would form preferably oligomers, owing to the steric restriction imposed by adjacent globular domains.

transmission electron microscopy (TEM) indicated that the incubated fusion protein assembled into a typical fibrillar amyloid-like structure, whereas DHFR-wt did not form any kind of assembly (Figure 1E,F). About 36.1 ± 4.2% of the original monomer in the solution was incorporated into fibrils at the end of the incubation reaction. The average size of the fibrils is 955 ± 75 nm, as measured by DLS. This is just a

https://dx.doi.org/10.1021/acs.biomac.0c01103
Biomacromolecules XXXX, XXX, XXX−XXX

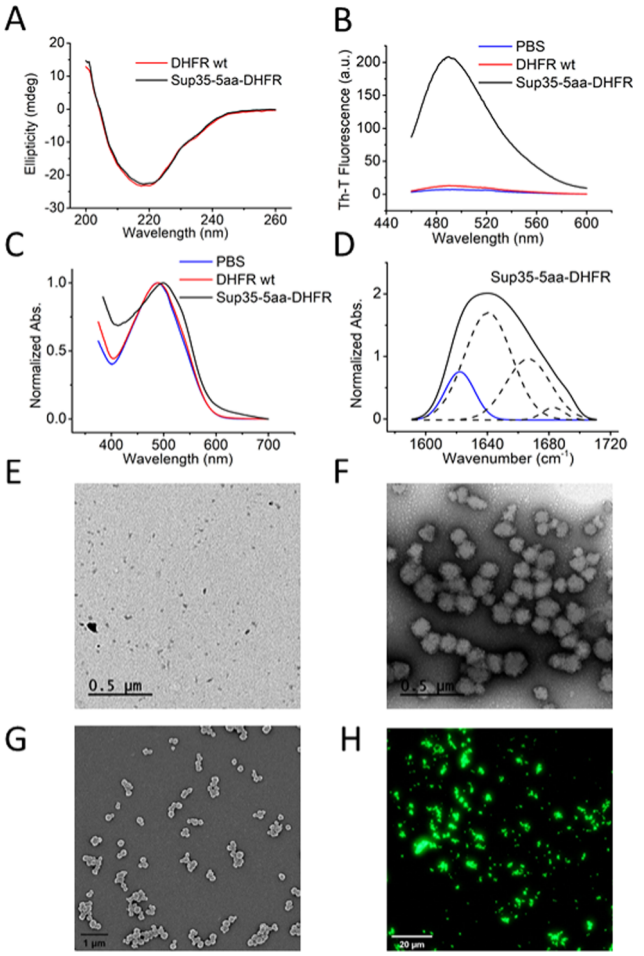

Figure 3. Characterization of soluble and aggregated Sup35-5aa-DHFR. (A) Far-UV CD spectra of soluble Sup35-5aa-DHFR and DHFR-wt, shown in black and red, respectively. Incubated Sup35-5aa-DHFR was analyzed by measuring Th-T fluorescence emission (B) and CR absorbance (C). DHFR-wt and Sup35-5aa-DHFR are shown in red and black, respectively. PBS without protein was included as a control (blue line). (D) FTIR absorbance spectra of incubated Sup35-8aa-DHFR in the amide I region of the spectrum (solid black line) and the component bands (dashed lines); the intermolecular β-sheet component is shown in blue. (E, F) Representative TEM micrographs of incubated proteins upon negative staining: (E) DHFR-wt and (F) Sup35-5aa-DHFR. Scale bar represents 500 nm. (G) Representative SEM micrograph of Sup35-5aa-DHFR particles. Scale bar represents 1 μm. (H) Fluorescence microscopy image of Sup35-5aa-DHFR particles incubated with fMTX. Scale bar represents 20 μm.

rough estimation of the fibrils' dimensions, since they are nonspherical particles.

To test if the DHFR enzyme keeps the native structure within the observed amyloid fibrils, we used a fluorescein-labeled version of MTX (fMTX), a competitive inhibitor that binds to the active site of DHFR. In the presence of the inhibitor, the amyloid fibrils appeared green, as visualized by fluorescence microscopy (Figure 1G), indicating that fMTX can bind to the catalytic site of the DHFR moieties embedded in these nanostructures.

Self-Assembly of Sup35-5aa-DHFR into Amyloid Oligomeric Nanoparticles. As shown above, a linker of eight residues suffices to allow the formation of infinite fibrils in which DHFR remains in its native conformation (Figure 2). Our recently derived model predicts that introducing a shorter

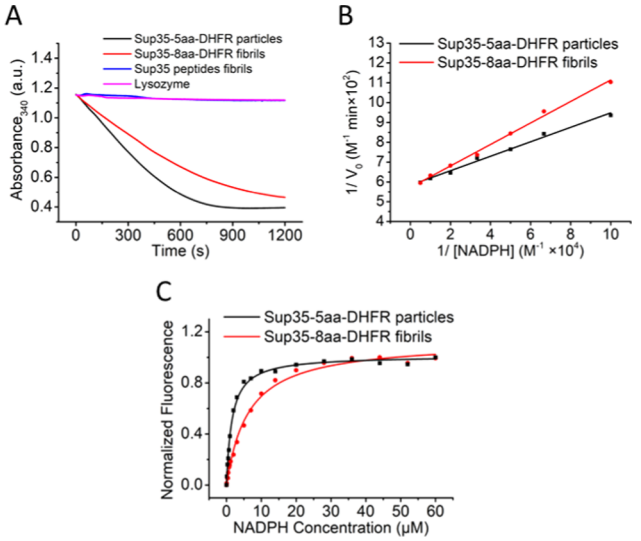

Figure 4. Catalytic activity and NADPH binding affinity of Sup35-5aa-DHFR particles and Sup35-8aa-DHFR fibrils. (A) The change in absorbance at 340 nm was monitored for each sample for 20 min in the presence of DHF and NADPH. Both assemblies were prepared at 100 nM. Sup35-SAC peptide fibrils and lysozyme are negative controls. (B) Lineweaver−Burk plot obtained by plotting the reciprocal of initial velocities of reactions against the reciprocal of the concentration of NADPH. (C) Measurement of K_d for NADPH binding to both assemblies by monitoring the quenching of DHFR intrinsic fluorescence. Fluorescence titrations were performed using 100 nM assemblies and the indicated concentrations of NADPH.

linker to connect the amyloidogenic and globular moieties would generate steric hindrance and might result in the formation of oligomeric structures, instead of fibrils (Figure 2).[16] To experimentally demonstrate this hypothesis, we constructed a Sup35-5aa-DHFR fusion, in which we connected Sup35-SAC and DHFR with a 5-residue linker consisting of SGSGS (Figure S2A,B).

Again, the protein was well-expressed (71 mg·L^{-1}) and soluble (Figure S2C). Purified Sup35-5aa-DHFR displayed a conformation very similar to that of DHFR-wt in solution, as assessed by far-UV CD (Figure 3A). The protein was incubated at 37 °C for four days, rendering Th-T (Figure 3B) and CR (Figure 3C) positive assemblies, with detectable intermolecular β-sheet contents (Figure 3D and Table S1). TEM imaging evidenced that, despite these amyloid-like properties, and in contrast to Sup35-8aa-DHFR, Sup35-5aa-DHFR assembles into spherical nanoparticles, which is consistent with an amyloid oligomeric nature (Figure 3E,F). The presence of spherical structures in the incubated Sup35-5aa-DHFR solution was further confirmed by scanning electron microscopy (SEM) (Figure 3G). About 40.2 ± 3.3% of the original monomer in the solution was incorporated into nanoparticles at the end of the incubation reaction.

The particles were very homogenous in size, with diameters of 147 ± 20 and 159 ± 24 nm as measured by TEM and SEM, respectively. These sizes are in good agreement with the 150 ± 50 nm measured for the particles in solution by dynamic light scattering (DLS) (Figure S4). Incubation of this sample with fMTX rendered green fluorescent aggregates (Figure 3H), indicating that, as in the amyloid fibrils, the inhibitor can bind to folded DHFR domains in the structure of the oligomeric protein nanoparticles. Therefore, as predicted, playing with the linker length allowed us to tune the assemblies' mesoscopic

https://dx.doi.org/10.1021/acs.biomac.0c01103
Biomacromolecules XXXX, XXX, XXX−XXX

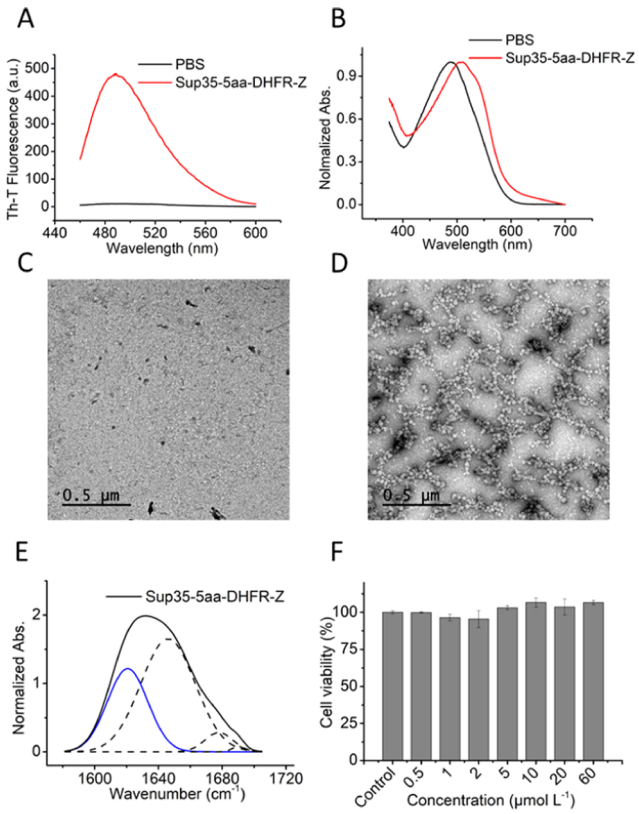

Figure 5. Characterization of aggregated Sup35-5aa-DHFR-Z. Incubated Sup35-5aa-DHFR-Z was analyzed by measuring the Th-T fluorescence emission (A) and CR absorbance (B). Sup35-5aa-DHFR-Z is shown in red; PBS without protein was included as a control (black line). Representative TEM micrographs of soluble Sup35-5aa-DHFR-Z (C) and incubated Sup35-5aa-DHFR-Z. (D) Scale bar represents 500 nm. (E) FTIR absorbance spectra of incubated Sup35-5aa-DHFR-Z in the amide I region of the spectrum (solid black line) and the component bands (dashed lines); the intermolecular β-sheet component is shown in blue. (F) Cytotoxicity of incubated Sup35-5aa-DHFR-Z. Results are expressed as means ± standard deviation (SD), n = 3, and analyzed using a one-way ANOVA test. The statistical differences between the control group and the test group were established at $P < 0.05$.

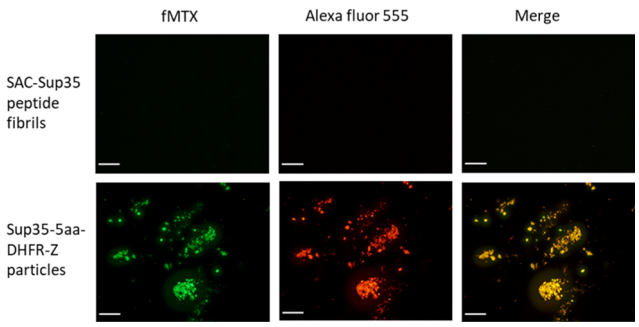

Figure 6. Dual-binding activity of Sup35-5aa-DHFR-Z nanoparticles. Representative fluorescence microscopy images of SAC-Sup35 peptide fibrils (upper panel) and Sup35-5aa-DHFR-Z nanoparticles (lower panel) incubated with fMTX (fluorescein, green channel) and an anti-EGFR antibody (Alexa fluor 555, red channel). Scale bar represents 50 μm.

properties and produce, for the first time, amyloid-like active spherical nanoparticles.

Catalytic Activity of DHFR in Fibrils and Nanoparticles. DHFR catalyzes the reduction of dihydrofolate (DHF) to tetrahydrofolate (THF) in the presence of reduced nicotinamide adenine dinucleotide phosphate (NADPH).[27] The binding of fMTX to fibrils and nanoparticles suggested that DHFR might keep its enzymatic activity in both kinds of assemblies. To further confirm this extent and evaluate the impact of each superstructure on the activity of the enzyme, we measured the catalytic activity of fibrils and nanoparticles at 100 nM in the presence of DHF and NADPH. We recorded the absorbance change at 340 nm for 20 min and plotted the resulting traces (Figure 4A). For both fibrils and nanoparticles, the decrease of NADPH absorbance with time indicates that they are catalytically active, whereas the fibrils formed by the Sup35-SAC peptide alone or lysozyme, used as negative controls, do not affect the NADPH absorbance at 340 nm. Importantly, the signal decreased faster for the nanoparticles than for the fibrils, which suggested that the smaller assemblies were more active, assuming that the proportion of properly folded DHFR moieties is similar in both assemblies.

Next, we sought to determine the apparent kinetic constants for both amyloid-like assemblies. We measured the initial velocities of the reactions in the presence of NADPH in a range of concentrations from 10 to 200 μM, while the concentration of DHF was fixed at 20 μM. Then, we calculated the kinetic constants from the resulting Lineweaver−Burk plots (Figure 4B and Table S2). The nanoparticles' V_{max} was 1712 ± 25 nM·min^{-1}, which does not differ significantly from that of the fibrils (V_{max} = 1745 ± 21 nM·min^{-1}). This was expected since the NADPH binding site and the catalytic center of DHFR should keep the same conformation in both assemblies. However, the nanoparticles exhibited a lower K_m (6.23 ± 0.32 μM) than that of the fibrils (9.44 ± 0.41 μM). This translates into a higher specificity constant for the nanoparticles (K_{cat}/K_m = 0.23 ± 0.01 μM^{-1}·s^{-1}) (Table S2).

The thermodynamic dissociation constants (K_d) for binding of NADPH to both assemblies were measured by monitoring the quenching of the DHFR intrinsic fluorescence (Figure 4C). The obtained values indicated that the binding affinity of nanoparticles for NADPH (K_d = 1.58 ± 0.07 μM) was 4-fold higher than that of the fibrils, with a K_d value of 6.26 ± 0.44 μM (Table S2). Thus, both the K_m and K_d constants indicate that the higher catalytic activity of the nanoparticles results from a higher NADPH binding capability of DHFR when embedded in the spherical amyloid-like structures, likely because the cofactor binding site is more accessible in these assemblies or, alternatively, because the proportion of conformationally active DHFR molecules is higher in the particles than in the fibrils.

Overall, the activity, homogeneity, stability, spherical structure, and moderate size of the novel oligomeric amyloid-like nanoparticles we describe here seem optimal for their exploitation as functionalized nanomaterials.

Building Up Sup35-5aa-DHFR-Z Bifunctional Nanoparticles. We sought to exploit the ability of Sup35-5aa-DHFR to form spherical structures of defined size to build up bifunctional nanoparticles with potential applications in targeted delivery. To this aim, we incorporated the Z-domain of *S. aureus* protein A (SpA) at the C-terminus of Sup35-5aa-DHFR through a flexible SG_2SG linker, to obtain the Sup35-5aa-DHFR-Z tripartite fusion protein (Figure S5A,B). The Z-domain is an engineered analog of the B-domain, one of the five homologous IgG-binding domains of SpA.[28] It consists of

https://dx.doi.org/10.1021/acs.biomac.0c01103
Biomacromolecules XXXX, XXX, XXX−XXX

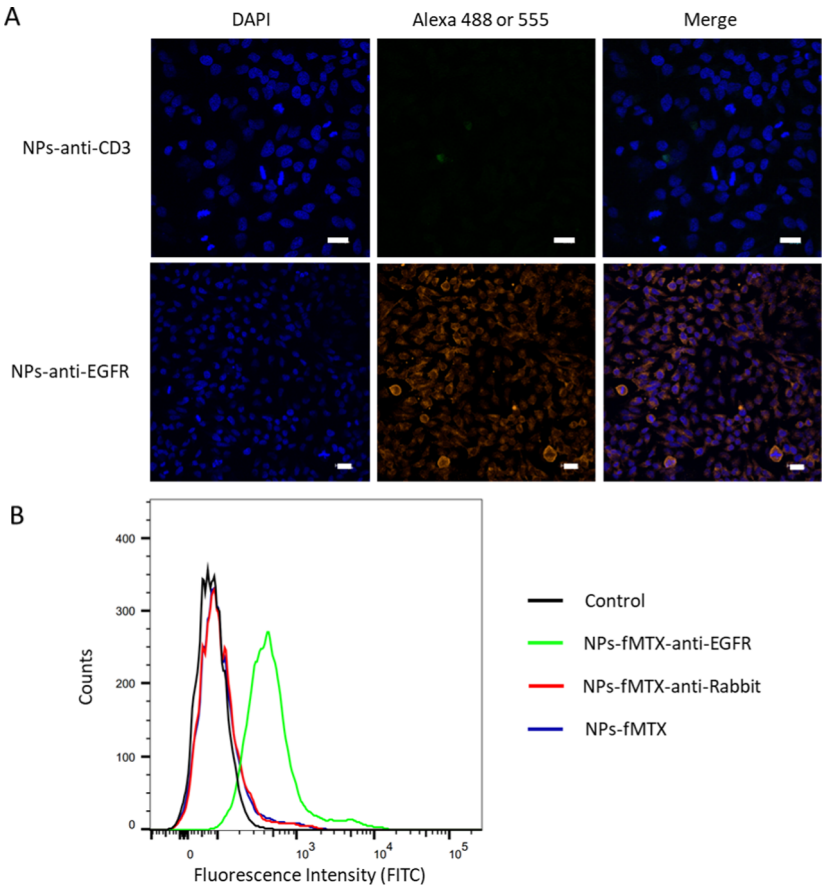

Figure 7. Binding specificity of functionalized Sup35-5aa-DHFR-Z nanoparticles to HeLa cells. (A) Representative confocal microscopy images of HeLa cells incubated with nanoparticles conjugated with an anti-CD3 antibody (NPs-anti-CD3, Alexa 488) (upper panel) or an anti-EGFR antibody (NPs-anti-EGFR, Alexa 555) (lower panel). Scale bar represents 20 μm. (B) Quantitative analysis of fluorescein fluorescence on HeLa cells by flow cytometry. HeLa cells were incubated with fMTX, anti-EGFR-loaded nanoparticles (NPs-fMTX-anti-EGFR, green line), fMTX and goat antirabbit antibody-loaded nanoparticles (NPs-fMTX-antirabbit, red line), and fMTX-loaded nanoparticles (NPs-fMTX, blue line). HeLa cells treated with PBS were used as a control. Fluorescein-labeled MTX (fMTX) was used as a fluorescence probe to calculate the proportion of cancer cells bound to nanoparticles using an FITC detector.

58 residues (6.5 kDa) and folds into a bundle-like shape composed of three α-helices. The Z-domain binds with high affinity to the Fc region of antibodies from different species and subclasses. The idea was that if Sup35-5aa-DHFR-Z assembles into amyloid nanoparticles, we might decorate them with any antibody of interest.

Once more, the protein was well-expressed (80 mg·L^{-1}) and soluble (Figure S5C). Once purified, we incubated the fusion protein at 37 °C for four days and assessed whether it binds to Th-T and CR. Again, the increase in Th-T fluorescence emission (Figure 5A) and the red shift of the CR absorbance (Figure 5B) were indicative of an amyloid-like structure. The band at 1620 cm^{-1} in the deconvoluted FTIR absorbance spectra confirmed the presence of the intermolecular β-sheet structure (Figure 5E and Table S1). Finally, TEM images showed that Sup35-5aa-DHFR-Z self-assembled into spherical particles (Figure 5D), whereas the soluble, nonincubated, tandem fusion protein did not form any assembly (Figure 5C). The size of such oligomers, as measured by TEM, was 43.6 ± 2.8 nm, in good agreement with the 40.1 ± 5.8 nm measured by DLS. Higher-magnification TEM images showed the high homogeneity and regular round shape of these nanoparticles (Figure S6). The size of these nanostructures is ∼1/3 of that formed by Sup35-5aa-DHFR. This reduction in size can be univocally attributed to the presence of the Z-domain. Sup35-5aa-DHFR-Z is ∼6 kDa larger than Sup35-5aa-DHFR; thus, if we assume that the two nanoparticles display similar compactness, this necessarily implies that the number of molecules in Sup35-5aa-DHFR-Z particles is significantly smaller. This reduction in size upon increasing the dimension of the adjacent domain was already predicted by the above-described relationship between AR and adjacent globular domains.[15] The larger the molecule appended to the AR, the lower the number of units that can be incorporated into the amyloid-like oligomers, and the smaller the size of the resulting particle.

Sup35-5aa-DHFR-Z Bifunctional Nanoparticles are Biocompatible. One of the main limitations of using amyloid-like materials in biomedical applications is that they might possess cytotoxic activity.[29] To discard this possibility, we tested the cytotoxicity of the Sup35-5aa-DHFR-Z nanoparticles at different concentrations, ranging from 0.5 to 60 μM, using the PrestoBlue assay (Figure 5F). The statistical analysis using a one-way ANOVA test indicated that the particles did not exhibit significant toxicity for human HeLa cells, suggesting that they would have excellent biocompatibility.

Dual-Binding Activity of Sup35-5aa-DHFR-Z Nanoparticles. To confirm that both DHFR and the Z-domain keep their native structure and functionality in Sup35-5aa-

https://dx.doi.org/10.1021/acs.biomac.0c01103
Biomacromolecules XXXX, XXX, XXX−XXX

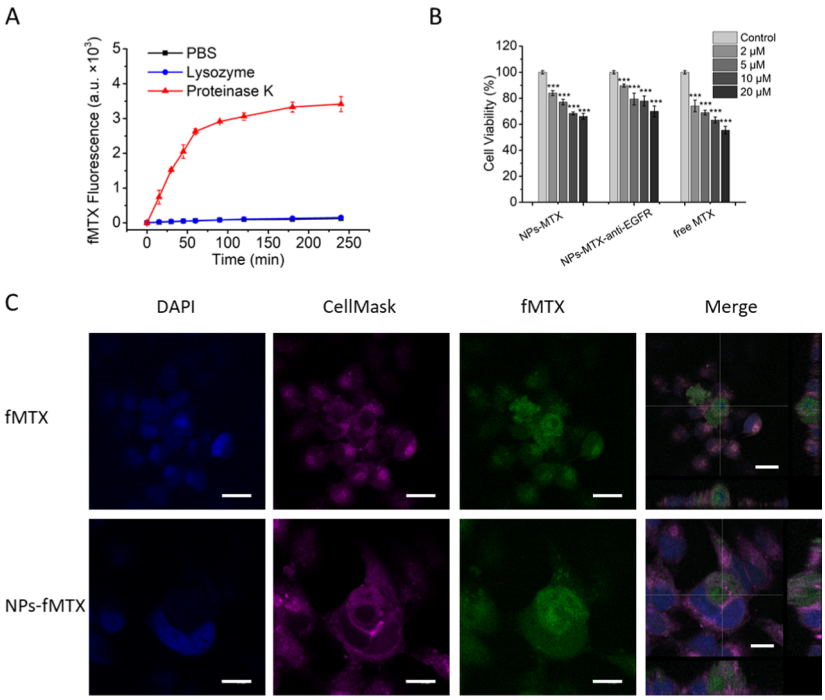

Figure 8. Release, uptake, and cytotoxicity of MTX in Sup35-5aa-DHFR-Z nanoparticles. (A) In vitro release of fluorescein-labeled MTX from Sup35-5aa-DHFR-Z nanoparticles in PBS buffer in the presence of 1 μg·mL^{-1} proteinase K (red line) at 37 °C (n = 2). The fluorescence emission of fMTX at 515 nm in the supernatant was measured at the indicated time points. Nanoparticles treated with PBS (black line) and lysozyme (blue line) were used as negative controls. (B) Viability of HeLa cells in the presence of free MTX, MTX-loaded nanoparticles (NPs-MTX), or MTX- and anti-EGFR-loaded nanoparticles (NPs-MTX-anti-EGFR). PBS buffer was used as a control. A final concentration of 5 ng·mL^{-1} proteinase K was added to the medium to mimic the proteinase-enriched microenvironment of tumors. Results are expressed as means ± SD (n = 3) and analyzed using a one-way ANOVA test. The statistical differences between the control group and the test group were established at $P < 0.001$. (C) Representative confocal images of HeLa cells incubated with free fMTX or fMTX-loaded nanoparticles (NPs-fMTX) preincubated with proteinase K. Nuclei were stained with DAPI, and membranes were stained with CellMask Deep Red. Fluorescein-labeled MTX (fMTX) was detected in the FITC channel. Scale bar represents 10 μm.

DHFR-Z nanoparticles, we incubated them with fMTX (green fluorescence) and an anti-EGFR antibody labeled with Alexa fluor 555 (red fluorescence). Then, they were precipitated and washed three times to remove any unbound molecule and resuspended in PBS buffer. When imaged using fluorescence microscopy, the particles appeared green and red in the respective channels, and the two signals overlapped when the channels were merged (Figure 6). This indicated that the DHFR and the Z-domain embedded in the spherical nanoparticles were bound to fMTX and the antibody, respectively. In contrast, the fibrils formed by the SAC-Sup35 peptide alone did not bind any of the two molecules, confirming that the observed binding to Sup35-5aa-DHFR-Z nanoparticles does not result from an unspecific interaction of the reagents with the common amyloid-like structure.

Sup35-5aa-DHFR-Z-Functionalized Nanoparticles Target Cancer Cells Specifically. We assessed if Sup35-5aa-DHFR-Z nanoparticles can target specific antigens in living cells once they have been loaded with antibodies through their multiple Z-domains. Nanoparticles loaded with red-labeled anti-EGFR antibody (NPs-anti-EGFR) were incubated with HeLa cells, which are known to overexpress EFGR at their membranes.[30] As can be observed in Figure 7A, confocal microscopy fluorescence images indicated that the vast majority of the cells were red fluorescent and, therefore, that the multivalent NPs-anti-EGFR had recognized them. In contrast, when the Sup35-5aa-DHFR-Z nanoparticles were loaded with a green-labeled anti-CD3 antibody and incubated with HeLa cells, no cellular labeling was detected, consistent with the fact that this cell type does not express the CD3 complex. Thus, the data indicated that the recognition of HeLa cells by NPs-anti-EGFR was antibody-driven and specific.

Next, we loaded Sup35-5aa-DHFR-Z nanoparticles, with both fMTX and anti-EGFR antibody (NPs-fMTX-anti-EGFR), with fMTX and a secondary goat antirabbit antibody (NPs-fMTX-antirabbit), or only with fMTX (NPs-fMTX), and we added the three functionalized protein nanoparticles to HeLa cell cultures. After washing the cells with PBS, they were immediately analyzed by flow cytometry, monitoring the green fluorescence of fMTX, present in all three nanoparticles, with an FITC emission detector. Only HeLa cells treated with NPs-fMTX-Anti-EGFR exhibited fMTX fluorescence (Figure 7B), whereas no significant fluorescence was detected for HeLa cells treated with NPs-fMTX-antirabbit or NPs-fMTX. Flow cytometry is quantitative, and the analysis indicated that >70% of the cells were bound to NPs-fMTX-anti-EGFR, which shows a high binding affinity of the functionalized nanoparticles for EGFR expressing cells. Indeed, confocal images of cells incubated with NPs-fMTX-anti-EGFR indicated that they target the cell membrane (Figure S7).

Overall, it appears that Sup35-5aa-DHFR-Z nanoparticles provide a modular strategy to target any cell type of interest, just by incorporating the adequate antibody thanks to their strong interaction with the properly folded Z-domains and the multivalency of the assembly.

https://dx.doi.org/10.1021/acs.biomac.0c01103
Biomacromolecules XXXX, XXX, XXX−XXX

Proteinase-Controlled Release of MTX from Sup35-5aa-DHFR-Z Nanoparticles. Cancer cells secrete a significant number of proteinases, including metalloproteinases,[31] serine proteinases,[32] and cathepsins.[33] This feature has been exploited to develop proteinase-responsive nanocarriers[34] and polymer nanoshells.[35]

It is known that amyloid fibrils are highly resistant to proteolysis, but we hypothesized that the globular domains hanging from the amyloid core in Sup35-5aa-DHFR-Z nanoparticles would be protease-sensitive. This will open an opportunity to use the DHFR moiety as a carrier for MTX under the assumption that the inhibitor will be released from the oligomers once they arrive at a protease-rich environment and the accessible DHFR domains would be proteolytically attacked.

We incubated fMTX-loaded nanoparticles with the broad-spectrum proteinase K (PK) at a final concentration of 1 μg·mL^{-1} and measured the kinetics of fluorescein fluorescence apparition in the supernatant, upon centrifugation (Figure 8A). The nanoparticles were incubated also in PBS alone or treated with lysozyme at the same concentration to ensure that any observed release is not spontaneous or unspecific. In contrast to control samples, PK-treated nanoparticles showed a continuous delivery of fMTX to the solution, with a cumulative release efficiency >90% after 4 h of reaction.

An SDS-PAGE of the nanoparticles indicated that they were SDS-sensitive since, despite high molecular species being observed, the vast majority of the fusion protein ran as a monomer. This sensitivity to the detergent is typical of amyloid oligomers.[36] This allowed us to follow the PK digestion by SDS-PAGE, which confirmed that the nanoparticles are proteinase-sensitive and that no intact Sup35-5aa-DHFR-Z fusion remains after 45 min and neither does any fragment compatible with an intact DHFR domain (Figure S8), explaining why fMTX is released from the protein nanoparticles.

Internalization of MTX Released from Loaded Nanoparticles. We investigated if the DHFR inhibitor released from NPs-fMTX can be uptaken by HeLa cells. To this aim, we incubated the cells with 10 μM free fMTX or fMTX-loaded nanoparticles, both preincubated with 50 ng·mL^{-1} PK for 5 min, followed by protease inactivation with EDTA. After 4 h of incubation, the medium was removed, and the cells were washed with the medium three times. Then, cells were stained with DAPI and CellMask Deep Red for nuclei and membrane visualization, respectively. Intracellular green fluorescent fMTX was observed by confocal microscopy for both free added fMTX and NPs-fMTX (Figure 8C), indicating that the nanoparticle-released inhibitor is efficiently internalized.

MTX-Loaded Nanoparticles Induce Death of Cancer Cells. We have demonstrated that the MTX-loaded nanoparticles can liberate DHFR-bound MTX and that the inhibitor can internalize into cancer cells. This immediately suggested that MTX-loaded nanoparticles could induce proteolysis-mediated cell death. Therefore, we measured the viability of HeLa cells in the presence of NPs-MTX, NPs-MTX-anti-EGFR, or free MTX. A final concentration of 5 ng·mL^{-1} PK was added to the cell culture medium to mimic the proteinase-enriched microenvironment of tumor tissues. In all cases, a significant dose-dependent decrease in HeLa cell viability was observed, compared with control cells incubated with PK only (Figure 8B). The concentration of proteinase in the assay is lower than the one described in the tumors' extracellular environment;[37] still, it is sufficient to promote MTX release from the nanoparticles, internalization of the inhibitor, and cancer cell death. Importantly, untreated and PK-treated Sup35-5aa-DHFR-Z nanoparticles are not toxic for nontumoral lung MRC-5 cells (Figure S9), indicating that the multifunctional nanoparticles might be safe for normal cells in vivo.

CONCLUSIONS

In the present work, we first demonstrated that by modulating interdomain linker length, one could attain a tight control of the mesoscopic properties of the resulting amyloid-like nanostructures. This strategy does not require intricate structural engineering since it relies on fundamental biophysical principles. The approach allowed us to generate oligomeric amyloid-like nanoparticles. These spherical nanoparticles are homogenous in size, stable, and biocompatible. Besides, the multiple globular domains they contain are highly active in the assembled state, as shown here for DHFR and the Z-domain. Therefore, they constitute a novel kind of functional and functionalizable nanomaterial.

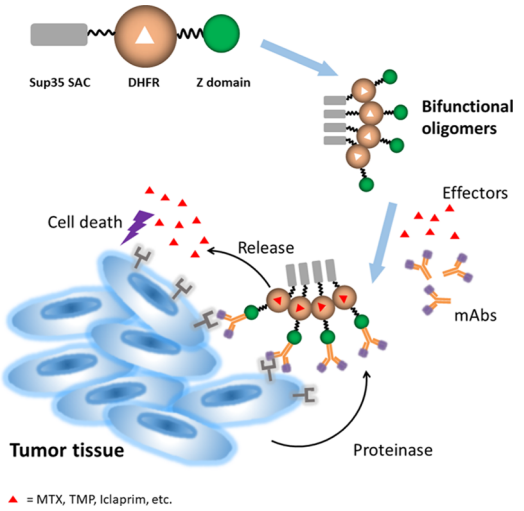

Figure 9. Schematic illustration of bifunctional amyloid oligomeric nanoparticles and their potential application for targeted drug delivery. The construct consists of the Sup35 soft amyloid core (Sup35-SAC, gray square), dihydrofolate reductase (DHFR, orange circle), and the Z-domain derived from protein A (green circle). The short linker between Sup35-SAC and DHFR enables the fusion protein to self-assemble into stable bifunctional oligomeric nanoparticles. Drugs (red triangles) and monoclonal antibodies (mAbs) loaded into the nanoparticles would target the tumor cells and release the drugs in a proteinase-enriched environment. As a consequence, the released drugs are internalized and induce the death of the targeted tumor cells.

We provide a proof-of-concept of the utility of these de novo-designed nanostructures by showing how they can be decorated with an antibody of interest, which act as an antenna, directing the multivalent nanoparticles to the specific cell types expressing the selected antigen at their surfaces, allowing the discrimination between diseased and functional cells. When this ability is combined with the capability of DHFR to carry and shield MTX, avoiding nonspecific toxic effects, it appears as a very appealing strategy for targeted delivery of the drug in the proteinase-enriched microenvironment of tumors, which is followed by MTX internalization into

https://dx.doi.org/10.1021/acs.biomac.0c01103
Biomacromolecules XXXX, XXX, XXX−XXX

the cytosol and localized killing of cancer cells (Figure 9). Overall, the multifunctional, self-assembled amyloid nanoparticles we present here constitute a new and safe nanotechnological modular scaffold with the potential of facilitating the specific delivery of agents to specific sites in the body, overpassing the major barrier for bioimaging and tissue-targeted therapies. Importantly, the building blocks of these nanostructures can be produced at high yield and purified at homogeneity from the soluble cell fraction, which results in reduced costs when compared with alternative nanomedicines.

■ ASSOCIATED CONTENT

Supporting Information

The Supporting Information is available free of charge at https://pubs.acs.org/doi/10.1021/acs.biomac.0c01103.

Characterization of fusion proteins; FTIR spectrum of DHFR-wt; DLS size distribution of the different assemblies; high-magnification TEM image of Sup35-5aa-DHFR-Z nanoparticles; confocal microscopy images of HeLa cells incubated with nanoparticles; SDS-PAGE analysis of proteinase K digestion; viability of MRC-5 cells; assignment of secondary structure components in the FTIR spectra; kinetics and thermodynamic dissociation constants of the assemblies (PDF)

■ AUTHOR INFORMATION

Corresponding Author

Salvador Ventura − *Institut de Biotecnologia i Biomedicina and Departament de Bioquímica i Biologia Molecular, Universitat Autònoma de Barcelona, 08193 Bellaterra, Spain;* orcid.org/0000-0002-9652-6351; Phone: 34-93-5868956; Email: salvador.ventura@uab.es; Fax: 34-93-5811264

Authors

Weiqiang Wang − *Institut de Biotecnologia i Biomedicina and Departament de Bioquímica i Biologia Molecular, Universitat Autònoma de Barcelona, 08193 Bellaterra, Spain;* orcid.org/0000-0002-6962-8811

Rafayel A. Azizyan − *Centre de Recherche en Biologie cellulaire de Montpellier, UMR 5237 CNRS, Université Montpellier, Montpellier 34090, France; Institut de Biologie Computationnelle, Université Montpellier, Montpellier 34090, France*

Adriana Garro − *Universidad Nacional de San Luis IMASL-CONICET, San Luis D5702, Argentina*

Andrey V. Kajava − *Centre de Recherche en Biologie cellulaire de Montpellier, UMR 5237 CNRS, Université Montpellier, Montpellier 34090, France; Institut de Biologie Computationnelle, Université Montpellier, Montpellier 34090, France;* orcid.org/0000-0002-2342-6886

Complete contact information is available at: https://pubs.acs.org/10.1021/acs.biomac.0c01103

Notes

The authors declare no competing financial interest.

■ ACKNOWLEDGMENTS

We acknowledge the technical support from the Cell Culture Unit of Servei de Cultius Cel·lulars i Producció d'Anticossos i Citometria (SCAC) and from the Servei de Microscopia of Universitat Autònoma de Barcelona (UAB). This work was funded by the Spanish Ministry of Economy and Competitiveness BIO2016-78310-R to S.V and by ICREA, ICREA-Academia 2015, to S.V. W.W. acknowledges financial support from the China Scholarship Council (CSC): No. 201606500007.

■ REFERENCES

(1) Knowles, T. P.; Mezzenga, R. Amyloid Fibrils as Building Blocks for Natural and Artificial Functional Materials. *Adv. Mater.* **2016**, *28*, 6546−6561.

(2) Ross, C. A.; Poirier, M. A. Protein Aggregation and Neurodegenerative Disease. *Nat. Med.* **2004**, *10*, S10−S17.

(3) Fowler, D. M.; Koulov, A. V.; Balch, W. E.; Kelly, J. W. Functional Amyloid−from Bacteria to Humans. *Trends Biochem. Sci.* **2007**, *32*, 217−224.

(4) Wei, G.; Su, Z.; Reynolds, N. P.; Arosio, P.; Hamley, I. W.; Gazit, E.; Mezzenga, R. Self-Assembling Peptide and Protein Amyloids: from Structure to Tailored Function in Nanotechnology. *Chem. Soc. Rev.* **2017**, *46*, 4661−4708.

(5) Rufo, C. M.; Moroz, Y. S.; Moroz, O. V.; Stöhr, J.; Smith, T. A.; Hu, X.; DeGrado, W. F.; Korendovych, I. V. Short Peptides Self-Assemble to Produce Catalytic Amyloids. *Nat. Chem.* **2014**, *6*, 303−309.

(6) Chiti, F.; Dobson, C. M. Protein Misfolding, Amyloid Formation, and Human Disease: A Summary of Progress Over the Last Decade. *Annu. Rev. Biochem.* **2017**, *86*, 27−68.

(7) Wang, W.; Navarro, S.; Azizyan, R. A.; Baño-Polo, M.; Esperante, S. A.; Kajava, A. V.; Ventura, S. Prion Soft Amyloid Core Driven Self-Assembly of Globular Proteins into Bioactive Nanofibrils. *Nanoscale* **2019**, *11*, 12680−12694.

(8) Sant'Anna, R.; Fernández, M. R.; Batlle, C.; Navarro, S.; De Groot, N. S.; Serpell, L.; Ventura, S. Characterization of Amyloid Cores in Prion Domains. *Sci. Rep.* **2016**, *6*, No. 34274.

(9) Sabate, R.; Rousseau, F.; Schymkowitz, J.; Ventura, S. What Makes a Protein Sequence a Prion? *PLoS Comput. Biol.* **2015**, *11*, No. e1004013.

(10) Sabate, R.; Rousseau, F.; Schymkowitz, J.; Batlle, C.; Ventura, S. Amyloids or Prions? That is the Question. *Prion* **2015**, *9*, 200−206.

(11) Wasmer, C.; Schütz, A.; Loquet, A.; Buhtz, C.; Greenwald, J.; Riek, R.; Böckmann, A.; Meier, B. H. The Molecular Organization of the Fungal Prion HET-s in its Amyloid Form. *J. Mol. Biol.* **2009**, *394*, 119−127.

(12) Baxa, U.; Cassese, T.; Kajava, A. V.; Steven, A. C. Structure, Function, and Amyloidogenesis of Fungal Prions: Filament Polymorphism and Prion Variants. *Adv. Protein Chem.* **2006**, *73*, 125−180.

(13) Li, J.; McQuade, T.; Siemer, A. B.; Napetschnig, J.; Moriwaki, K.; Hsiao, Y.-S.; Damko, E.; Moquin, D.; Walz, T.; McDermott, A.; et al. The RIP1/RIP3 Necrosome Forms a Functional Amyloid Signaling Complex Required for Programmed Necrosis. *Cell* **2012**, *150*, 339−350.

(14) Chen, A. K.-H.; Lin, R. Y.-Y.; Hsieh, E. Z.-J.; Tu, P.-H.; Chen, R. P.-Y.; Liao, T.-Y.; Chen, W.; Wang, C.-H.; Huang, J. J.-T. Induction of Amyloid Fibrils by the C-terminal Fragments of TDP-43 in Amyotrophic Lateral Sclerosis. *J. Am. Chem. Soc.* **2010**, *132*, 1186−1187.

(15) Azizyan, R. A.; Garro, A.; Radkova, Z.; Anikeenko, A.; Bakulina, A.; Dumas, C.; Kajava, A. V. Establishment of Constraints on Amyloid Formation Imposed by Steric Exclusion of Globular Domains. *J. Mol. Biol.* **2018**, *430*, 3835−3846.

(16) Kajava, A. V.; Baxa, U.; Wickner, R. B.; Steven, A. C. A Model for Ure2p Prion Filaments and Other Amyloids: The Parallel Superpleated β-Structure. *Proc. Natl. Acad. Sci. U.S.A.* **2004**, *101*, 7885−7890.

(17) Azizyan, R. A.; Wang, W.; Anikeenko, A.; Radkova, Z.; Bakulina, A.; Garro, A.; Charlier, L.; Dumas, C.; Ventura, S.; Kajava, A. V. Amyloidogenicity as a Driving Force for the Formation of Functional Oligomers. *J. Struct. Biol.* **2020**, *212*, No. 107604.

(18) Schnell, J. R.; Dyson, H. J.; Wright, P. E. Structure, Dynamics, and Catalytic Function of Dihydrofolate Reductase. *Annu. Rev. Biophys. Biomol. Struct.* **2004**, *33*, 119−140.

(19) Tashiro, M.; Tejero, R.; Zimmerman, D. E.; Celda, B.; Nilsson, B.; Montelione, G. T. High-Resolution Solution NMR Structure of the Z Domain of Staphylococcal Protein A. *J. Mol. Biol.* **1997**, *272*, 573−590.

(20) Forsgren, A.; Sjöquist, J. "Protein A" from *S. aureus*: I. Pseudo-immune Reaction with Human γ-globulin. *J. Immunol.* **1966**, *97*, 822−827.

(21) Huffman, D. H.; Wan, S. H.; Azarnoff, D. L.; Hoogstraten, B. Pharmacokinetics of Methotrexate. *Clin. Pharmacol. Ther.* **1973**, *14*, 572−579.

(22) Blaney, J. M.; Hansch, C.; Silipo, C.; Vittoria, A. Structure-Activity Relationships of Dihydrofolated Reductase Inhibitors. *Chem. Rev.* **1984**, *84*, 333−407.

(23) Qindeel, M.; Khan, D.; Ahmed, N.; Khan, S.; Rehman, A. U. Surfactant-Free, Self-Assembled Nanomicelles-Based Transdermal Hydrogel for Safe and Targeted Delivery of Methotrexate against Rheumatoid Arthritis. *ACS Nano* **2020**, *14*, 4662−4681.

(24) Sadrjavadi, K.; Shahbazi, B.; Fattahi, A. De-Esterified Tragacanth-Chitosan Nano-Hydrogel for Methotrexate Delivery; Optimization of the Formulation by Taguchi Design. *Artif. Cells, Nanomed., Biotechnol.* **2018**, *46*, 883−893.

(25) Tawfik, M. K. Combination of Coenzyme Q10 with Methotrexate Suppresses Freund's Complete Adjuvant-Induced Synovial Inflammation with Reduced Hepatotoxicity in Rats: Effect on Oxidative Stress and Inflammation. *Int. Immunopharmacol.* **2015**, *24*, 80−87.

(26) Choi, G.; Kim, T.-H.; Oh, J.-M.; Choy, J.-H. Emerging Nanomaterials with Advanced Drug Delivery Functions; Focused on Methotrexate Delivery. *Coord. Chem. Rev.* **2018**, *359*, 32−51.

(27) Bystroff, C.; Oatley, S. J.; Kraut, J. Crystal structures of *Escherichia coli* dihydrofolate reductase: The NADP + holoenzyme and the Folate. cntdot. NADP+ Ternary Complex. Substrate Binding and a Model for the Transition State. *Biochemistry* **1990**, *29*, 3263−3277.

(28) Moks, T.; ABRAHMSÉN, L.; NILSSON, B.; HELLMAN, U.; SJÖQUIST, J.; UHLÉN, M. Staphylococcal Protein A Consists of Five IgG-Binding Domains. *Eur. J. Biochem.* **1986**, *156*, 637−643.

(29) Díaz-Caballero, M.; Navarro, S.; Ventura, S. Soluble Assemblies in the Fibrillation Pathway of Prion-Inspired Artificial Functional Amyloids are Highly Cytotoxic. *Biomacromolecules* **2020**, *21*, 2334−2345.

(30) Laskin, J. J.; Sandler, A. B. Epidermal Growth Factor Receptor: A Promising Target in Solid Tumours. *Cancer Treat. Rev.* **2004**, *30*, 1−17.

(31) Folgueras, A. R.; Pendas, A. M.; Sanchez, L. M.; Lopez-Otin, C. Matrix Metalloproteinases in Cancer: From New Functions to Improved Inhibition Strategies. *Int. J. Dev. Biol.* **2004**, *48*, 411−424.

(32) Koshikawa, N.; Yasumitsu, H.; Umeda, M.; Miyazaki, K. Multiple Secretion of Matrix Serine Proteinases by Human Gastric Carcinoma Cell Lines. *Cancer Res.* **1992**, *52*, 5046−5053.

(33) Koblinski, J. E.; Dosescu, J.; Sameni, M.; Moin, K.; Clark, K.; Sloane, B. F. Interaction of Human Breast Fibroblasts with Collagen I Increases Secretion of Procathepsin B. *J. Biol. Chem.* **2002**, *277*, 32220−32227.

(34) Zhu, L.; Kate, P.; Torchilin, V. P. Matrix Metalloprotease 2-Responsive Multifunctional Liposomal Nanocarrier for Enhanced Tumor Targeting. *ACS Nano* **2012**, *6*, 3491−3498.

(35) Yang, J.; Yang, Y.; Kawazoe, N.; Chen, G. Encapsulation of Individual Living Cells with Enzyme Responsive Polymer Nanoshell. *Biomaterials* **2019**, *197*, 317−326.

(36) Gadad, B. S.; Britton, G. B.; Rao, K. Targeting Oligomers in Neurodegenerative Disorders: Lessons from α-Synuclein, Tau, and Amyloid-β Peptide. *J. Alzheimer's Dis.* **2011**, *24*, 223−232.

(37) Schmalfeldt, B.; Prechtel, D.; Härting, K.; Späthe, K.; Rutke, S.; Konik, E.; Fridman, R.; Berger, U.; Schmitt, M.; Kuhn, W. Increased Expression of Matrix Metalloproteinases (MMP)-2, MMP-9, and the Urokinase-type Plasminogen Activator is Associated with Progression from Benign to Advanced Ovarian Cancer. *Clin. Cancer. Res.* **2001**, *7*, 2396−2404.

https://dx.doi.org/10.1021/acs.biomac.0c01103
Biomacromolecules XXXX, XXX, XXX−XXX